bioRxiv preprint doi: https://doi.org/10.1101/2024.06.13.598939; this version posted June 14, 2024. The copyright holder for this preprint (which was not certified by peer review) is the author/funder. All rights reserved. No reuse allowed without permission.

Expanding salivary biomarker detection by creating a synthetic neuraminic acid sensor via chimeragenesis

Samuel J. Verzino[1], Sharona A. Priyev[1], Valeria A. Sánchez Estrada[1], Gemma X. Crowley[1], Alexandra Rutkowski[1], Amelia C. Lam[1], Elizabeth S. Nazginov[1], Paola Kotemelo[1], Agustina Bacelo[1,2], Desiree T. Sukhram[1], Frank X. Vázquez[2], Javier F. Juárez[1]

[1]Dept. of Biological Sciences and [2]Dept. of Chemistry, Saint John's University, 8000 Utopia Parkway, Queens, NY (USA)

bioRxiv preprint doi: https://doi.org/10.1101/2024.06.13.598939; this version posted June 14, 2024. The copyright holder for this preprint (which was not certified by peer review) is the author/funder. All rights reserved. No reuse allowed without permission.

ABSTRACT

Accurate and timely diagnosis of oral squamous cell carcinoma (OSCC) is crucial in preventing its progression to advanced stages with a poor prognosis. As such, the construction of sensors capable of detecting previously established disease biomarkers for the early and non-invasive diagnosis of this and many other conditions has enormous therapeutic potential. In this work, we apply synthetic biology techniques for the development of a whole-cell biosensor (WCB) that leverages the physiology of engineered bacteria *in vivo* to promote the expression of an observable effector upon detection of a soluble molecule. To this end, we have constructed a bacterial strain expressing a novel chimeric transcription factor (Sphnx) for the detection of N-acetylneuraminic acid (Neu5Ac), a salivary biomolecule correlated with the onset of OSCC. This WCB serves as the proof-of-concept of a platform that can eventually be applied to clinical screening panels for a multitude of oral and systemic medical conditions whose biomarkers are present in saliva.

bioRxiv preprint doi: https://doi.org/10.1101/2024.06.13.598939; this version posted June 14, 2024. The copyright holder for this preprint (which was not certified by peer review) is the author/funder. All rights reserved. No reuse allowed without permission.

INTRODUCTION

Biosensors are detection systems resulting from an analytical approach in which biological elements convert a physicochemical stimulus into a detectable signal[1]. Among them, Whole Cell Biosensors (WCBs) - detection systems in which a physiologically active cell sustains an array of biomolecular elements (receptors, channels, enzymes, regulators, etc.) capable of detecting and processing a signal and produce a detectable output - stand out due to their versatility and engineering potential[1]. Microbial WCBs in particular have shown their potential in fields ranging from environmental monitorization and food testing, to medical applications[2]. Microorganisms can grow rapidly in relatively inexpensive media and produce all the necessary biological elements for analyte detection. Unlike conventional sensors that may require large and complex instruments and laborious sample processing, WCBs can detect a bioavailable substance directly from the environment with minimal preparation, enabling their incorporation into *in situ* detection methods that can revolutionize point-of-care early detection diagnosis[3].

WCBs benefit from the synergies resulting from the combination of native systems, evolved during millions of years to detect the miscellany of molecules surrounding microbes, with the ever growing toolkit that synthetic biology provides (such as the creation of synthetic genetic circuits[4–7]). Frequently, the presence of a soluble analyte becomes associated with a conformational change of a protein, so that its binding state to DNA gets altered, modifying the transcription profile of a regulated reporter[8]. These transcription factor (TF)-based WCBs benefit the most from the use of monogenic transcriptional repressors[4,5], control systems encoded by a single gene whose product prevents transcription in the absence of a small soluble inducer molecule. The catalog of characterized TFs capable of interacting with small soluble molecules is expanding yet still limited[9]. The advent of synthetic biology has enabled us to better understand

bioRxiv preprint doi: https://doi.org/10.1101/2024.06.13.598939; this version posted June 14, 2024. The copyright holder for this preprint (which was not certified by peer review) is the author/funder. All rights reserved. No reuse allowed without permission.

protein modularity such that we can better engage in regulator customization and *de novo* creation, to expand the panoply of molecules that can be detected[10,11]. In this paper, we centered our efforts on the detection of a salivary biomarker that, to the best of our knowledge, was not the inducer of any characterized TF.

Human saliva contains a vast array of metabolites informative of oral and systemic health[12], making its continuous sampling by benchtop, portable, and wearable equipment extremely coveted. A dental practice able to utilize such sampling technologies may increase its role at the forefront of early disease prevention and diagnosis. Electrochemical intraoral biodevices capable of detecting salivary biomarkers presently exist, yet they are limited in the scope of molecules they detect and lack adaptability to sense new ones[13]. Bioengineering solutions enabling point-of-care diagnostics will greatly benefit patients by improving at-home health monotorization[14]. Diagnostic screenings that do not require invasive procedures (i.e. a blood sample or a biopsy) are preferred by patients, which makes saliva a prime biological fluid candidate to be sampled for health and disease markers[15,16]. In this work we focused our attention on N-acetylneuraminic acid (neuraminic acid, Neu5Ac), the most common of the sialic acids originally isolated from salivary glands[17–19]. Neu5Ac fulfills key roles in human physiology[20] as well as in commensal and pathogenic bacteria[17]. Moreover, changes in salivary sialylation might become a suitable early indicator of changes associated with malignant pathologies, given their correlation to periodontal disease (PD) and oral squamous cell carcinoma (OSCC)[21]. The oral microbiome of patients with PD include bacteria such as *Tannerella forsythia*, which engage in glycan harvesting behavior: they cleave Neu5Ac molecules from glycoproteins to stealthily evade their host's immune system[22]. Additionally, abnormally high concentrations of Neu5Ac have been associated with the onset of oral cancer[23,24]: a group of neoplasms which affect any region in the oral cavity, pharynx, and

bioRxiv preprint doi: https://doi.org/10.1101/2024.06.13.598939; this version posted June 14, 2024. The copyright holder for this preprint (which was not certified by peer review) is the author/funder. All rights reserved. No reuse allowed without permission.

salivary glands[25]. Oral cancer is often used interchangeably with oral squamous cell carcinoma (OSCC), which accounts for more than 90% of oral malignant epithelial neoplasms[25]. As one of the most prevalent cancers in the world[26], untreated OSCC has very poor prognosis and, as such, early detection is essential for successful treatment remission[27]. Recently, it has also been proposed that salivary Neu5Ac could interfere with SARS-Cov-2 (COVID-19) infection, acting as a competitive inhibitor blocking the viral antigens recognized by the host receptors[28]. Each of these factors made quantification of salivary Neu5Ac a desirable target for detection by biosensors.

The absence of a native TF capable of detecting Neu5Ac motivated us to construct a synthetic monogenic repressor for its integration in a synthetic circuit that would enable the strain bearing it to behave as a WCB. We favor these regulators due to their simplicity, compact nature, and ease of integration into synthetic circuits[4,5,29]. The process of constructing our custom Neu5Ac-sensing regulators is based on streamlined gene fusion / chimeragenesis methods developed by our laboratory to detect soluble molecules[10] . Here, we describe a Neu5Ac TF-based WCB that employs engineered bacterial machinery to fulfill the functions of the three basic modules present in any detection system: a sensing module, a processing unit, and an actuator. The living WCB can intake a Neu5Ac signal by expressing a novel synthetic transcription factor, Sphnx, that bridges detection and processing. A separate reporter plasmid completes the system providing a gene encoding a fluorescent protein (sfGFP, henceforth stylized as GFP) whose expression is regulated by the synthetic TF Sphnx so that detectable changes in fluorescence occur upon the detection of soluble Neu5Ac. Sphnx is a member of a new combinatorial library of TFs assembled via a simplified chimeragenesis process. Important clues on inter-domain communication of modular proteins have started to be gathered by comparing Sphnx to non-functional members of the TF collection. Protein tertiary structure modeling of functional and non-

bioRxiv preprint doi: https://doi.org/10.1101/2024.06.13.598939; this version posted June 14, 2024. The copyright holder for this preprint (which was not certified by peer review) is the author/funder. All rights reserved. No reuse allowed without permission.

functional regulators has contributed to establish comparisons between them helping to elucidate intricate and frequently difficult to predict dynamics that may condition the success or failure of any chimeric TF.

RESULTS AND DISCUSSION

Design and Construction of Synthetic Transcription Factors. The functionality of the WCBs that we have built in this work hinges on the obtention of a TF capable of binding Neu5Ac with efficacy and precision. The Neu5Ac-induced monogenic transcriptional repressor we intended to assemble included three modules: a N-terminus (N_t) DNA Binding Domain (DBD), a linker sequence (LNK), and a C-terminus (C_t) Ligand Binding Domain (LBD). The DBD specifically recognizes an operator sequence in the promoter it regulates, driving the expression of the reporter gene (*sfgfp*). The LBD is tasked with the recognition of Neu5Ac, providing specificity to the TF. Finally, the LNK sequence act as a bridge, providing the right amount of flexibility / rigidity necessary for information transfer between DBD and LBD: steric changes in the LBD associated with Neu5Ac binding get translated into steric changes in the DBD effecting a change of its oligomeric state that results in the unbinding of the TF from its operator and thus in a de-repression of transcription. By using a gene fusion / chimeragenesis approach we generated a library of repressors with a common N_t-DBD-LNK-LBD-C_t architecture.

Our selected DBD was sourced from the paradigm of transcriptional regulators: the *lac* repressor or LacI[30]. Though naturally induced by lactose / IPTG, we exclusively employ the DBD of LacI recognizing the operator *lacO* present in the P_{lac} promoter (as defined in[10]). We decided to use DBD-LacI because the *lac* repressor originated as a modular protein with two domains, and

bioRxiv preprint doi: https://doi.org/10.1101/2024.06.13.598939; this version posted June 14, 2024. The copyright holder for this preprint (which was not certified by peer review) is the author/funder. All rights reserved. No reuse allowed without permission.

has been previously used in the construction of several functional chimeras[31–33]. It is important to remark that the exclusive use of DBD-LacI, as opposed to the full protein, ensures that chimeric proteins carrying this domain will recognize their target operator, yet avoid responding to native inducers.

Candidate LBD selection is accomplished through bibliographical research. Since the LBD is the domain that recognizes the molecule of interest for which we build the biosensing strain, it can be sourced from any whole protein or protein domain as opposed to being co-opted from a previously documented regulator. One of our main sources of the LBDs we employ in our chimeragenesis pipeline are periplasmic binding proteins (PBPs)[34]. These are standalone subunits of transporters that share a common ancestor with the LBD domains of the LacI / GalR family of regulators[32]. To build the synthetic TF we required for this project, we needed to identify LBD candidates that strongly bind our soluble molecule of interest (Neu5Ac). PBPs SatA and SiaP were selected for their binding affinity and specificity for the transport of Neu5Ac. SatA is a product of the *satABCD* (*s*ialic *a*cid *t*ransport) operon that encodes an ATP Binding Cassette (ABC) transporter[35] from *Haemophilus ducreyi*[36]. An alternative *satABCD* system present in *Corynebacterium glutamicum* has been demonstrated to be essential for its growth using Neu5Ac as sole carbon source[37]. SiaP is a product of the *siaPQM* operon, which encodes a Tripartite ATP-independent periplasmic (TRAP) transporter in *Haemophilus influenzae*[38,39]. SiaP was the first TRAP-associated PBP whose structure was elucidated (*Vibrio cholerae*, *Pasteurella multocida* and *Fusobacterium nucleatum*[38,40]). Structural comparisons and thermodynamic studies of SatA and SiaP suggest that similar affinities for Neu5Ac are achieved in the two PBPs through distinct mechanisms: one enthalpically driven and the other entropically driven. SiaP, as well as other TRAP transporters, are hypothesized to command an enthalpically driven ligand binding strategy

bioRxiv preprint doi: https://doi.org/10.1101/2024.06.13.598939; this version posted June 14, 2024. The copyright holder for this preprint (which was not certified by peer review) is the author/funder. All rights reserved. No reuse allowed without permission.

due to the abundance of charged residues (Arg, Lys, Asp, and Glu) at their binding pocket. SatA, alternatively, is hypothesized to bind its substrate in what is considered an entropic approach because of the numerous hydrophobic and polar residues (Tyr, Phe, Gly, Leu, Asn, and Ser) at its binding pocket[41]. The structure of *H. influenzae* SiaP in the presence of Neu5Ac (PDB 3B50) reveals the ligand bound in a deep cavity with its carboxyl group forming a salt bridge with a highly conserved Arg residue[38]. Initial studies of SiaP isolated from *H. influenzae* displayed a binding K_d of ≈120 nM when affinity for Neu5Ac was tested[39]. Subsequent studies established a value closer to K_d ≈58 nM[38]. Similar binding affinity of SatA complexes has been identified with a K_d ≈133 nM[41]. The collection of empirical data supporting the ability of SatA and SiaP to bind Neu5Ac made them ideal candidates to become the LBD of a chimeric TF responsive to Neu5Ac.

The final piece of the chimeric gene puzzle consisted on establishing a connection between DBD and LBD domains. This task was performed by elements called linker (LNK) regions that tend to be less structured than the domains they connect[42]. In order to maximize the chances of transmitting the information of Neu5Ac binding to the DBD, so that it can detach from *lacO* and enable transcription, we decided to connect both domains via two different strategies: directly without a true LNK (condition identify as LNK1 for uniformity purposes) or by one out of four LNKs characterized by having different biophysical properties (identified as LNK2 to LNK5, *Supp. Table 1*). It is important to note that while LNK1 does not contain a true linker, the LBDs we chose, by virtue of being PBPs, are proteins that would be exported to the periplasm of the cell under natural circumstances, and thus contain a native signal peptide at their N-terminus. This kind of peptide appears to be unstructured for the most part, barring a short alpha-helix region[43]. We decided to include the signal peptides of both SiaP and SatA due to existent examples of functional chimeras containing similar structures, such as the glucose-inducible $SLCP_{GL}$[33] and the benzoate-

bioRxiv preprint doi: https://doi.org/10.1101/2024.06.13.598939; this version posted June 14, 2024. The copyright holder for this preprint (which was not certified by peer review) is the author/funder. All rights reserved. No reuse allowed without permission.

inducible CbnR-ABE44898-OD[10] TFs. At this stage, we had identified all the elements we needed to start assembling our new chimeric TFs.

dsDNA fragments encoding the DBD and all LNK-LBD variants were obtained as detailed in the *Materials and Methods* section. To initiate the construction of a library containing all the desired chimeric TFs, we performed several Gibson assembly reactions with all the domain-encoding fragments and linearized expression vector pUC19RBS, followed by transformation in NEB5-alpha competent cells. Resulting clones were isolated and individually sequenced. This approach was performed twice. Chimeric combinations that were not present in the libraries were re-attempted to be individually cloned five times with no success, at which point we proceeded to put pause to their construction and move the project forward, subcloning the TF collection we had generated up to that point in time into the low-copy vector pCKTRBS. It is important to note that the expression of any heterologous protein is *per se* taxing on bacterial metabolism, and that TFs might be especially burdensome[44,45]. Chimeric constructions including DBD-LacI and SiaP / SatA seem to provoke a certain toxicity to the cell, albeit to different degrees depending on the specific domain combination. Indirect evidence supporting this hypothesis was observed when constructions expressing the chimeric TFs were transformed into *E. coli* MC4100 to assess their behavior in M63 minimal media with glycerol as the sole carbon source. Under these resource-limited conditions, stressed bacteria have more difficulties in thriving, and MC4100 cells bearing pCKT-*Chimera* vectors displayed a very modest and erratic growth consistent with our assumptions (data not shown). *Table 1* contains the chimeric TFs built and assayed presented in this study, as well as a simplified interpretation of their functionality when grown in rich media.

Screening of transcription factors. A functional *in vivo* screening was implemented using GFP as reporter. Plasmid pHC_DYOLacI-R (*Supp. Table 2*) was transformed into candidate strains

bioRxiv preprint doi: https://doi.org/10.1101/2024.06.13.598939; this version posted June 14, 2024. The copyright holder for this preprint (which was not certified by peer review) is the author/funder. All rights reserved. No reuse allowed without permission.

194 expressing the chimeric TFs from pCKTRBS vectors under the control of TetR-aTc. This
195 constitutes a genetic circuit (*Figure 1a*) that enables a controlled expression of the chimera as well
196 as its controlled induction. This circuit behaves as a B-or-not-A universal two input gate[46] (*Figure*
197 *1b*), where there are two inputs (A, aTc supplementation; B, Neu5Ac supplementation) and one
198 output (detection of GFP fluorescence). Based on the addition of the inputs we can define three
199 states in the genetic circuit (*Figure 1c*): *Basal* (aTc^-/$Neu5Ac^-$), no input added, GFP is expressed
200 from its promoter in pHC_DYOLacI-R; *Repression* (aTc^+/$Neu5Ac^-$), the presence of aTc induces
201 TetR which is incapable of remaining attached to P_{tetO} and thus the chimera is expressed from its
202 pCKT vector repressing the expression of GFP; *De-repression* (aTc^+/$Neu5Ac^+$), the chimera is
203 expressed but if it is functional it is induced by Neu5Ac, de-repressing the promoter driving the
204 expression of GFP. By comparing the behavior of the strain expressing the aforementioned circuit
205 under these conditions, we can rule out non-functional synthetic TFs. In the case that the chimeric
206 protein was not a functional repressor, GFP-associated fluorescence could be detected in the
207 *Repression* state. On the other hand, if the chimera was able to bind to *lacO* on the reporter
208 promoter yet incapable to recognize Neu5Ac with its LBD, or to transmit a LBD to DBD
209 conformational change resulting in its detachment from the operator, we would have obtained a
210 functional super-repressor[47] unable to respond to its inducer and, thus, not a valid tool to detect
211 Neu5Ac. *Figure 1d* illustrates the expected GFP production along a growth curve for a strain
212 expressing the screening genetic circuit that included an ideal chimera. It is important to note that
213 even though Neu5Ac is a monosaccharide, its supplementation to growth media did not
214 significantly increase the OD_{600} of the assayed strains, at least up to the tested 10 mM concentration
215 (*Supp. Figure 1*). Regardless of this observation, GFP-associated fluorescence data displayed in
216 this publication is always expressed as relative fluorescence (arbitrary units) corrected by the

bioRxiv preprint doi: https://doi.org/10.1101/2024.06.13.598939; this version posted June 14, 2024. The copyright holder for this preprint (which was not certified by peer review) is the author/funder. All rights reserved. No reuse allowed without permission.

OD_{600} of the culture, in order to account for growth disparities among different strains and conditions. It is also important to note that repression by LacI, or LacI-derived chimeras, is rarely absolute so that a certain level of leakage, and thus of background reporter gene expression, is always expected to some extent[33,48].

All the chimeric TFs included in *Table 1* were screened for their ability to bind DNA and thus to repress the expression of the GFP reporter, as well as to be induced by Neu5Ac enabling production of the fluorescent protein. All members of the collection of MG1655 (pCKT-*Chimera*, pHC_DYOLacI-R) strains bearing the genetic circuit described in *Figure 1* were tested *in vivo* to assess their ability to behave as Neu5Ac biosensors. Among the chimeric proteins expressed by this strain collection we include the TF Lumos, which did not contain any of the expected no-linker / linker options but an unexpected 6 amino acid linker (LNK6) resulting from an abnormal assembly reaction in which the last 18 bases of *DBD-lacI* were duplicated (*Supp. Table 1*). Given the stable nature of the amino acid string, as well as our agnostic approach to which LNK sequence could be the best performing one, we decided to maintain this construction in our pool. TFs Kunst (LacI-LNK3-SiaP), Bastet (LacI-LNK5-SiaP), Harpy (LacI-LNK1-SatA), and Haus (LacI-LNK2-SatA) showed no de-repression abilities when Neu5Ac was supplemented. Further assaying their behavior, our attention was captured by Kunst. *Supp. Figure 2* shows the behavior of Kunst, which only exhibits a tendency to repress P_{lac} at the very beginning of a 40 h time course, yet after the 3 h mark does not show any difference between induced and uninduced conditions. A preliminary evaluation of the structural differences between Sphnx and Kunst is included in its own section of *Results and Discussion*. Another TF that presented an unexpected induction profile was Siren (LacI-LNK1-SiaP), which displayed an intriguing function as a proper repressor inducible by Neu5Ac but only in the stationary phase of growth (*Supp. Figure 3*). In the future we intend to

bioRxiv preprint doi: https://doi.org/10.1101/2024.06.13.598939; this version posted June 14, 2024. The copyright holder for this preprint (which was not certified by peer review) is the author/funder. All rights reserved. No reuse allowed without permission.

study this protein in depth, since its repression / de-repression profile is very attractive for a whole-cell biosensor setup in which a bacterial culture sustaining itself at stationary phase is continuously monitoring an input for an extended period of time. The TF Lumos (LacI-LNK6-SiaP) provided some preliminary data supporting its functionality, while a candidate biosensor strain expressing Sphnx (LacI-LNK2-SiaP) exhibited the most suitable repression and induction profile compatible with that of a TF capable of binding to Neu5Ac. Even though our sample size is extremely reduced - judging by the difficulty to obtain them as well as by their lack of functionality- SatA-based fusions seem to be less stable and more prone to Neu5Ac non-responsiveness. Further studies and the creation of bigger chimeric libraries, however, are required to confirm this hypothesis. At this injunction, we focused our efforts on better characterization of the most promising TF we had assembled: Sphnx.

In order to validate our preliminary observations, we systematically compared GFP production over time of MG1655 (pCKT-Sphnx, pHC_DYOLacI-R) cells expressing Sphnx either in the presence or absence of Neu5Ac. *Figure 2a* displays the results of time course experiments over a period of 25 hours. GFP production induced by the presence of Neu5Ac was observed from the first hour of growth, with the Neu5Ac-induced cultures showing a tendency to display higher fluorescence than repressed ones.

As a away to confirm these *in vivo* observations, we analyzed the induction of P_{lac} driving the expression of GFP in MG1655 (pCKT-Sphnx, pHC_DYOLacI-R) by qRT-PCR experiments performed as indicated in *Materials and Methods*. The expression levels of *sfgfp* calculated as the ratio of the induced condition over the repressed condition were 1.58 ± 0.24 ($n = 8$, error expressed as SEM) statistically significant and consistent with an induction of the expression in the presence

bioRxiv preprint doi: https://doi.org/10.1101/2024.06.13.598939; this version posted June 14, 2024. The copyright holder for this preprint (which was not certified by peer review) is the author/funder. All rights reserved. No reuse allowed without permission.

of Neu5Ac (*Supp. Figure 4a)*. However, the degree of induction varied widely across biological replicas (*Supp. Figure 4b)*.

Further *in vitro* experiments were also performed to confirm the interaction between P_{lac} and the DBD-LacI of Sphnx. Electrophoretic mobility shift assays (EMSA, *Materials and Methods*) showed that cell extracts from NEB5-alpha (pCKT-Sphnx) grown for 5 h were capable of retarding the migration of a P_{lac}-*sfgfp* probe compared to control extracts that were not expressing Sphnx (data not shown). Neu5Ac behaved as the inducer of Sphnx, since binding of the protein to the probe was diminished in a concentration-dependent manner in the presence of the sialic acid (*Figure 2b*). On the other hand, cell extracts from NEB5-alpha (pCKT-Siren) grown for 5 h were able to bind the probe but not to unbind in the presence of Neu5Ac, confirming our *in vivo* observations. Previous publications report a similar behaviour: DBDs from bacterial transcriptional repressors tend to retain their ability to bind to their operator sequences even when integrated in a new chimeric TF[49–51], another testimony to the high modularity of these proteins. Our initial *in vitro* DNA-protein interaction studies require future validation with purified chimeras in order to calculate the kinetics of the Sphnx-*lacO* and Sphnx-Neu5Ac-*lacO* interactions, yet they represent a promising step forward towards characterizing the interaction between our synthetic TF and its cognate operator.

At this juncture of the project, both *in vivo* and *in vitro* experiments strongly suggested that Sphnx was a transcriptional repressor capable of interacting with *lacO* and being de-repressed by neuraminic acid. To better understand the dynamics of the Sphnx-Neu5Ac interaction we analyzed the production of GFP by MG1655 (pCKT-Sphnx, pHC_DYOLacI-R) cultures at 14 hours of growth (*Materials and Methods*) when exposed to different concentrations of neuraminic acid around the average for an adult male (≈1 mM)[52]. The average fold difference of GFP expression

bioRxiv preprint doi: https://doi.org/10.1101/2024.06.13.598939; this version posted June 14, 2024. The copyright holder for this preprint (which was not certified by peer review) is the author/funder. All rights reserved. No reuse allowed without permission.

between the repressed and induced conditions was 2.25 ± 0.74 for cultures induced with 0.5 mM Neu5Ac, 2.54 ± 0.52 for cultures induced with 1.0 mM Neu5Ac, 3.81 ± 1.15 for cultures induced with 2.0 mM Neu5Ac, and 5.21 ± 2.00 for cultures induced with 5.0 mM Neu5Ac (n = 8, error expressed as SEM). These results were commensurable with those observed for $SLCP_{GL}$ (LacI-GGBP-OD)[33], as well as for CbnR-ABE44898-OD and LmrR-BzdB1_nSP[10], all of them modular chimeric TFs. *Figure 2c* shows the levels of GFP fluorescence observed in basal and repressed cultures as well as in cultures induced by 0.5, 1.0, 2.0 and 5.0 mM neuraminic acid. These assays corroborated that relative fluorescence between basal (aTc^-/$Neu5Ac^-$) and repressed (aTc^+/$Neu5Ac^-$) conditions were significant. Cultures in which the genetic circuit used to test Sphnx were de-repressed (aTc^+/$Neu5Ac^+$) displayed statistically significant values compared to the repressed cultures when in the presence of 1.0 mM and 2.0 mM Neu5Ac. Induction by 0.5 and 5.0 mM was not significant. It is important to note that relative fluorescence values in the 5.0 mM-induced biological replicas were widely dispersed, suggesting that an overabundance of Neu5Ac might interfere with the stability of the host strain producing some deleterious effect associated to the expression of the heterologous Sphnx and GFP proteins in the assayed conditions. These results showing Sphnx induction are promising, yet they underline the need to refine chimeric TFs resulting from the assembly of pre-existing modules to optimize their induction range as well as gene dose and reporter genes used to study their behaviour *in vivo* and *in vitro*. Newly created synthetic TFs tend to have limited transfer function and specificity, and thus to require further engineering for their field deployment in biosensors[53]. In this regard, we are optimistic about the future improvement of the chimeras we create: the estimated K_d of SiaP and SatA for neuraminic acid are in the nM range[38,39,41] (calculated *in vitro*), whereas in this work we present data in the mM range (*in vivo*). This suggests that we have not reached the full potential of our LBDs and

bioRxiv preprint doi: https://doi.org/10.1101/2024.06.13.598939; this version posted June 14, 2024. The copyright holder for this preprint (which was not certified by peer review) is the author/funder. All rights reserved. No reuse allowed without permission.

there is an opportunity to optimize Sphnx's structure to better benefit from the high specificity and affinity of our LBD. It is also important to note that Sphnx is currently at the same point in evolutionary history when DBD-LacI was fused to the ancestral version of its current LBD, long before communication between DBD and LBD had been refined and perfected by natural selection[32]. Regarding the use of alternative reporters that may shed more light on the induction profile of Sphnx, we acknowledge that the use of GFP has some inherent limitations for their use of prokaryotes (e.g. extremely varying maturation times dependent on strain and metabolic state[54]), which has motivated us to initiate the development of better reporting systems.

Modeling of the 3D structure of chimeric transcription factors. Another element we are starting to explore is the importance of linkers for the functionality of modular proteins, an often-neglected design element[55]. Since the beginning of our journey characterizing the chimeric TFs, we found extremely intriguing the fact that Sphnx (LacI-LNK2-SiaP, N_t-DBD-EKEKEK-LBD-C_t) and Kunst (LacI-LNK3-SiaP, N_t-DBD-GSGSGS-LBD-C_t), which are nearly identical proteins (*Supp. Materials Appendix*), possessed opposed behaviours when interacting with neuraminic acid. The recent release of AlphaFold 3[56] has enabled us to predict the structures of multimeric chimeric proteins in the presence of their dsDNA operator, allowing us to model the proteins under conditions closer to those found in actual WCBs. Sphnx and Kunst were both modeled as dimers using AlphaFold 3, along with a DNA double helix containing the *lacO* (5'-ATTGTGAGCGGATAACAATT-3' and its complementary sequence) recognized by the DBD-LacI they both carry. Our goal was to predict structures that could help explain why Sphnx binds Neu5Ac while Kunst does not, despite only differing by six amino acids. *Figure 3a* shows the predicted Kunst DBD (green) bound to the DNA double helix (gray) and the formation of a dimer between the PBP (cyan). The structure shows a mostly disordered linking region (orange),

bioRxiv preprint doi: https://doi.org/10.1101/2024.06.13.598939; this version posted June 14, 2024. The copyright holder for this preprint (which was not certified by peer review) is the author/funder. All rights reserved. No reuse allowed without permission.

including the GSGSGS (LNK3) linker (violet). The predicted Sphnx model (*Figure 3b*), on the other hand, shows that the connecting region adopts a helical structure, including the EKEKEK (LNK2) linker, and appears to form contacts between both the DBD and PBP. Rotating the Kunst structure by 90° (*Figure 3c*) we can observe that the GSGSGS (linker does not interact with the protein or DNA. In contrast, rotating the Sphnx structure by 90° (*Figure 3d*) further shows that the linker forms contacts between the DBD and PBP domains, with interactions occurring across different monomer chains. Further analysis shows that the helical linker in Sphnx forms electrostatic salt bridges between itself and both the DBD and PBP domains. *Figure 3e* shows the acidic residues on the linker (Glu) forming contacts with basic residues (Lys) on the DBD and PBP domains. Specifically, the predicted structure suggests that the residues expected to form salt bridges include Glu67-Lys2 on the DBD and Glu69-Lys152 on the PBP. These salt bridges likely stabilize the helical linker, affecting the flexibility and stability of the polypeptide, an effect that has been previously observed in other proteins[57]. From these predicted structures, we hypothesize that these salt bridges stabilize helicity in the flexible linker in a way that positively affects the PBP function by interacting with the DBD and the PBP, explaining the ligand binding functionality of Sphnx compared to non-binding Kunst protein. Zooming out to see the larger structure (*Figure 3f*), aromatic residues near the linker salt bridges are visible. These residues are key for testing the new predicted structures and designing new chimeric proteins in the future. We intend to purify Sphnx and Kunst to perform fluorescence analysis of the protein-ligand interactions, including fluorescence quenching and fluorescence anisotropy studies. The construction of 3D models, using the latest version of AlphaFold, will continue to enable us to explore which mutations might enhance ligand binding in a way that was previously unavailable, also allowing us to model conditions closer to the actual multimeric *in vivo* conditions.

bioRxiv preprint doi: https://doi.org/10.1101/2024.06.13.598939; this version posted June 14, 2024. The copyright holder for this preprint (which was not certified by peer review) is the author/funder. All rights reserved. No reuse allowed without permission.

CONCLUSIONS

This work presents MG1655 (pCKT-Sphnx, pHC_DYOLacI-R), the first iteration of a transcription factor-based whole-cell biosensor strain capable of detecting the salivary biomarker neuraminic acid and relay its presence through the production of a fluorescent reporter. The keystone of the genetic circuit enabling the detection of the soluble molecule is a new transcriptional repressor: Sphnx. The apparent absence of a native Neu5Ac-binding transcription factor led the authors to create a custom-made regulator via a straightforward synthetic biology approach that enables the generation of chimeras capable of repressing a known promoter and being de-repressed by a molecule of interest. Neuraminic acid is an attractive analyte to monitor since its enhanced levels in saliva are correlated with conditions that range from periodontal disease[52] (oral microbes harvest sialic acid to evade our immune system[22]) to the onset of oral squamous cell carcinoma[23,24]. To the best of our knowledge, Sphnx is the first published transcriptional repressor capable of being induced by neuraminic acid.

This study supports the idea that the ability to construct custom-made TFs, affordably and on-demand, is instrumental in expanding the panoply of small soluble molecules that can be detected by biosensors in a field limited by the availability of sensing modules[32]. It is important to note that synthetic TFs such as Sphnx are not the closing of a chapter, but the origin of a new source of regulators whose performance can be improved via directed engineering of their ligand binding pockets[58]. It is widely acknowledged that biosensor specificity and biosensor-analyte reaction curves need to be optimized for the practical application of the WCB[53]. Once the biosensor strain is optimized we will test it first on synthetic saliva[59] preparations with a gradient of Neu5Ac

bioRxiv preprint doi: https://doi.org/10.1101/2024.06.13.598939; this version posted June 14, 2024. The copyright holder for this preprint (which was not certified by peer review) is the author/funder. All rights reserved. No reuse allowed without permission.

concentrations and, eventually, with clinical salivary samples. The MG1655 (pCKT-Sphnx, pHC_DYOLacI-R) strain represents the first step in the obtention of a functional WCB for the detection of neuraminic acid, a necessary launchpad to achieve the goal of eventual clinical deployment of the sensor.

Conclusively, the modular assembly of fusion genes sheds light on the importance of inter-domain communication for multi-domain protein functionality[60]. Our study presents the interesting contrast between the inducibility of Sphnx as opposed to Kunst, and particularly the unexpected role that a potential LBD-mediated stabilization of the linker may play in the de-repressibility of the TF dimer. *In vitro* assays using purified proteins, as well as further modeling simulation analysis and, eventually, the crystallization of these proteins will contribute in illuminating the complex dynamics necessary for modular proteins to fulfill their function.

In summary, this work presents a new biosensor for N-acetylneuraminic acid, a salivary biomarker relevant to oral health, which is based on a synthetic TF whose construction contributes to illuminating the role of different domains in the functionality of modular proteins.

bioRxiv preprint doi: https://doi.org/10.1101/2024.06.13.598939; this version posted June 14, 2024. The copyright holder for this preprint (which was not certified by peer review) is the author/funder. All rights reserved. No reuse allowed without permission.

MATERIALS AND METHODS

Bacterial strains and growth conditions. Bacterial strains and plasmids used are listed in *Supp. Table 2*. *E. coli* strains were grown at 37°C in LB (Lysogenic Broth[61]) medium unless otherwise indicated. When required, *E. coli* cells were grown in M63 minimal medium[62] using the necessary nutritional supplements and 30 mM glycerol (Sigma, St. Louis, MO) as a carbon source. Antibiotics were added at the following concentrations: 100 $\mu g \cdot ml^{-1}$ ampicillin/carbenicillin and 25 $\mu g \cdot ml^{-1}$ chloramphenicol (Sigma, St. Louis, MO). For protein expression from pCKTRBS-derived vectors, cultures were induced with 0.5 $\mu g \cdot ml^{-1}$ anhydrotetracycline (aTc) (Clontech, Mountain View, CA). When experimental conditions required it, cultures were supplemented with N-acetylneuraminic acid (neuraminic acid, Neu5Ac; Sigma, St. Louis, MO) at a 1 mM concentration unless otherwise indicated.

Culture growth was routinely monitored in a BioPhotometer D30 (BioSpectrometer Basic Kinetic and Fluorescence; Eppendorf, Hamburg, Germany). When it was required, bacterial growth and GFP production were recorded in a Varioskan LUX Multimode Microplate Reader (Thermo Fisher, Waltham, MA). Cultures were pipetted on a 96-well plate (Flat bottom Polystyrene Black with clear bottom; Corning, Corning, NY) covered with a Breathe-Easy BEM-1 gas-permeable membrane (Diversified Biotech, Dedham, MA) and incubated in a plate reader, where OD_{600} and fluorescence in the range of GFP (excitation 485 nm, emission 528 nm) were either tracked along time courses (up to 40 h) or subjected to point measurements. NEB5-alpha (pHC_DYOLacI-R) and MG1655 were included in every plate as GFP-positive and GFP-negative reference strains, respectively. For standard time course experiments, overnight precultures of the strains were used to inoculate (starting OD_{600} 0.025) fresh growth media (supplemented with aTc and Neu5Ac when indicated) in 96-well plates (180 µl total volume per well). For single point measurements,

bioRxiv preprint doi: https://doi.org/10.1101/2024.06.13.598939; this version posted June 14, 2024. The copyright holder for this preprint (which was not certified by peer review) is the author/funder. All rights reserved. No reuse allowed without permission.

overnight precultures of the strains (plus aTc and Neu5Ac when required) were used to inoculate 5 ml of fresh media supplemented in the same manner as the precultures. After 14 h of growth, 180 µl samples of the cultures were transferred to 96-well plates to enable OD_{600} and fluorescence readings.

Statistical analysis as well as data visualization were performed with R (https://www.r-project.org/) in the RStudio (RStudio Inc., Boston, MA) and Visual Studio Code environments (Microsoft Corp., Redmond, WA).

Molecular biology techniques. Molecular biology techniques were performed following commonly used standard protocols and as per manufacturers' instructions[63]. PCR reactions took place in a 6321 Mastercycler PRO Vapo Protect Thermal Cycler (Eppendorf, Hamburg, Germany). Routine separation of DNA and RNA in agarose gels was performed in an RunOne Electrophoresis system (EmbiTec, San Diego, CA). Agarose gels were imaged in an UVP UVSolo Touch (Analytic Jena, Jena, Germany). Plasmid DNA was purified with a Qiaprep Spin Miniprep Kit (Qiagen, Hilden, Germany). DNA fragments were purified with DNA Clean-up and Concentration Kit (Zymo research, Irvine, CA). The oligonucleotides employed for PCR amplification of the cloned fragments and other molecular biology techniques are summarized in *Supp. Table 3* and were supplied by IDT (Coralville, IA). All cloned inserts and DNA fragments were confirmed either via Sanger sequencing[64] performed by Azenta Inc. (Burlington, MA), or Oxford-Nanopore whole-plasmid sequencing performed by Plasmidsaurus (Eugene, OR). Commercially available NEB5-alpha chemically competent cells (NEB, Ipswich, MA) were used for routine transformations. Alternatively, electrocompetent *E. coli* cells were generated and transformed immediately (Gene Pulser; Bio-Rad, Hercules, CA)[63]. Nucleotide sequence analyses were done at the National Center for Biotechnology Information server (www.ncbi.nlm.nih.gov) and Benchling Biology Software

bioRxiv preprint doi: https://doi.org/10.1101/2024.06.13.598939; this version posted June 14, 2024. The copyright holder for this preprint (which was not certified by peer review) is the author/funder. All rights reserved. No reuse allowed without permission.

(www.benchling.com). Cloning was routinely performed via Gibson assembly[65] unless otherwise indicated.

Domain selection and cloning. DBD-LacI is located on *lacI* 5' region, from the start codon to base 198, encoding a peptide of 66 amino acids that comprises the N-terminus of our chimeric proteins. This domain was obtained via PCR amplification from plasmid pCKTRBS-LacIwt[10] using the oligonucleotide pair SV00001 / SV00002. SatA from *H. ducreyi* (Uniprot Q7VL18) and SiaP from *H. influenzae* (Uniprot P44542) were ordered as synthetic dsDNA fragments (IDT, Coralville, IA). Several variants of the LBDs SatA and SiaP were amplified via PCR so that they would include 5' overhangs including linkers (LNK2-5) or no linker whatsoever (LNK1). SatA was amplified with primers SV00030-SV00034 / SV00004 and SiaP with primers SV00015-SV00019 / JFJ0018.

Genes encoding the chimeric TFs were originally assembled in pUC19[66]. The vector was amplified via divergent PCR with primers JFJ00019 / JFJ00020, which introduce a consensus RBS for *E. coli*, originating plasmid pUC19RBS. Tripartite Gibson assemblies including linear pUC19RBS, DBD-LacI, and LNK-LBD were performed and the resulting constructions transformed into NEB5-alpha competent cells. After a carbenicillin selection in solid media, a subset of the resulting clones was isolated and their plasmids (pUC19-*Chimera* family, *Supp. Table 2*) purified and sequenced to validate the presence of chimeric TFs. The resulting TF genes cloned into pUC19RBS were amplified using SV00024 / SV00025 for SiaP-derived chimeras and SV00024 / SV00026 for their SatA counterparts. These primers amplify our TF genes from the 5' DBD-LacI, just downstream of the consensus RBS site, to the stop codon of the LBD. Low copy plasmid pCKTRBS[10] was amplified via divergent PCR using primer pairs SV00022 / SV00021 for SiaP-derived chimeras and SV00022 / SV00023 for their SatA counterparts. These primers introduce 5'

bioRxiv preprint doi: https://doi.org/10.1101/2024.06.13.598939; this version posted June 14, 2024. The copyright holder for this preprint (which was not certified by peer review) is the author/funder. All rights reserved. No reuse allowed without permission.

and 3' overhang sequences providing homology to our dsDNA chimeric gene fragments, and including in their 5' side our consensus RBS site. Bipartite Gibson assemblies including linear pCKTRBS and the fusion genes encoding the chimeras were performed, and the resulting assembly products transformed into NEB5-alpha competent cells. After a carbenicillin selection in solid media, resulting clones were isolated and their plasmids sequenced to confirm the presence of chimera-encoding genes. Resulting pCKT-*Chimera* plasmids were purified from NEB5-alpha (pCKT-*Chimera*) strains and electroporated into MG1655 cells. After confirming the presence of the plasmid in the new host, MG1655 (pCKT-*Chimera*) were electroporated with the reporter plasmid pHC_DYOLacI-R. Validated MG1655 (pCKT-*Chimera*, pHC_DYOLacI-R) strains were used for *in vivo* and *in vitro* analysis of the functionality of the novel chimeric TFs. The sequences of all the oligonucleotides used in this work can be found in *Supp. Table 3*.

Electrophoretic mobility shift assay (EMSA). In order to obtain cell extracts enriched in the Sphnx / Siren proteins, NEB5-alpha (pCKT-Sphnx) and NEB5-alpha (pCKT-Siren) cells were grown on LB supplemented with aTc for 5 hours at 37˚C in a shaker incubator. Cells were recovered by centrifugation at 4°C (15' at 4,000 g) and then resuspended in 20 mM Tris-HCl (pH 7.0) to be sonicated at 70 amp for 30 seconds (30 cycles of 1 second; Branson Digital Sonifier, Danbury, CN). A subsequent centrifugation at 4°C (20' at 20,000 g) was performed to eliminate cell debris from the sample. The recovered supernatant was then incubated with the DNA probe, a 251 bp dsDNA fragment amplified from plasmid pHC_DYOLacI-R with primers SV00028 / SV00029, containing P_{lac} (including *lacO*). Cell extract (5 µl) and DNA probe (5 µl) were incubated together with reaction buffer (20% glycerol, 100 mM KCl, 500 $\mu g \cdot ml^{-1}$ bovine serum albumin, 20mM Tris-HCl pH 7.5). The reaction mixture is incubated for 30' at 30 ˚C. After incubation of the retardation mixtures, 2 µl of Gel loading dye without SDS (NEB, Ipswich, MA)

bioRxiv preprint doi: https://doi.org/10.1101/2024.06.13.598939; this version posted June 14, 2024. The copyright holder for this preprint (which was not certified by peer review) is the author/funder. All rights reserved. No reuse allowed without permission.

were added to each reaction. Mixtures were subsequently fractionated by electrophoresis in precast 6% polyacrylamide gels (Novex TBE Gels; Invitrogen, Waltham, MA) buffered with 0.5X TBE (45 mM Tris borate, 1mM EDTA). Gels were run at constant voltage (100 V) for 90' in a Mini Gel Tank (Invitrogen, Waltham, MA) and afterwards stained for 1 h in 50 ml of 0.5X TBE buffer supplemented with 5 µl of SYBR Gold dye (Invitrogen, Waltham, MA) while gently shaken. Post staining, gels were imaged in a UVP UVSolo Touch (Analytic Jena, Jena, Germany).

qRT-PCR analysis. Quantitative Real Time Polymerase Chain Reaction (qRT-PCR) was used to assay the transcription of our reporter gene (*sfgfp*). MG1655 (pCKT-*Chimera*, pHCDYOLacI-R) strains were precultured overnight in of 3 ml LB supplemented with the corresponding selection antibiotics. On the next day, 100 µl of overnight preculture were used as inoculum for several cultures, 10 ml each, of fresh LB (plus selection antibiotics). Each one of the cultures was supplemented so that it would represent one of these three different conditions: *Basal* (aTc^-, $Neu5Ac^-$), *Repressed* (aTc^+,$Neu5Ac^-$), and *De-repressed* (aTc^+, $Neu5Ac^+$). Where experimental conditions required it, cultures were supplemented with 0.5 $\mu g \cdot ml^{-1}$ anhydrotetracycline (aTc) (Clontech, Mountain View, CA) and 1 mM neuraminic acid (Neu5Ac; Sigma, St. Louis, MO). For every independent qRT-PCR experiment, three biological replicates were created across each of these three conditions. These cultures were placed in a shaker incubator at 37˚C for 5 hours and pelleted at 4˚C and 4,000 g. Pellets were either frozen at -80˚C for future use or immediately processed for total RNA extraction. Cells from each individual pellet were set for lysis by resuspendion in 1 ml of IBI reagent, a phenol and guanidine isothiocyanate mixture (IBI Scientific, Dubuque, IA). 200 µl of chloroform (Fisher Scientific, Pittsburgh, PA) was added to the lysate and the mixture was vigorously shaken to homogeneity, followed by centrifugation (benchtop minifuge) at 4˚C and 14,500 rpm for 15 minutes that led to a phase separation. 500 µl of the upper

bioRxiv preprint doi: https://doi.org/10.1101/2024.06.13.598939; this version posted June 14, 2024. The copyright holder for this preprint (which was not certified by peer review) is the author/funder. All rights reserved. No reuse allowed without permission.

aqueous phase was mixed with an equal volume of 100% ethanol. At this point, total RNA was purified from DNA / RNA phase with Direct-zol RNA Miniprep Kit (Zymo Research, Irvine, CA) where the TRIzol reagent steps are replaced with the phenol and chloroform phase separation. Total RNA eluted with ddH_2O was then retrotranscribed using qScript Flex cDNA Synthesis Kit (QuantaBio, Beverly, MA). A volume totaling 1 µg RNA was incubated with random hexamers and then supplemented with retrotranscriptase enzyme mix to synthesize cDNA. cDNA resulting from the last step was used as a template for the amplification of a 256 bp fragment with oligonucleotides SV00027A / SV00027 in a CFX96 Real-Time PCR System (Bio-Rad, Hercules, CA). Primers had been designed to amplify a region of pHC_DYOLacI comprising the beginning of *sfgfp*, so that when the tested chimera was being expressed it repressed the expression of GFP unless Neu5Ac was present. Cq values were analyzed as a measure of gene expression using the ΔΔCq ($2^{-\Delta\Delta Ct}$) method[67].

Protein Structure Prediction using AlphaFold 3. The 3D structures of the target proteins, Sphnx (LacI-LNK2-SiaP, N_t-DBD-EKEKEK-LBD-C_t) and Kunst (LacI-LNK3-SiaP, N_t-DBD-GSGSGS-LBD-C_t), were predicted using AlphaFold 3[56], developed by Google DeepMind (London, UK). The predictions were performed using the publicly available AlphaFold 3 web server (https://golgi.sandbox.google.com/). Both Sphnx and Kunst proteins were modeled as dimers, along with the DNA double helix containing *lacO* (5'-ATTGTGAGCGGATAACAATT-3' and its complementary sequence). Post-prediction, the structures were visualized and further analyzed using VMD[68] to determine key protein-protein interactions.

bioRxiv preprint doi: https://doi.org/10.1101/2024.06.13.598939; this version posted June 14, 2024. The copyright holder for this preprint (which was not certified by peer review) is the author/funder. All rights reserved. No reuse allowed without permission.

Acknowledgments and Funding

This material is based upon work supported by St. John's University (SJU) via J.F.J.'s starting package as well as St. John's SEED grants (2020-2021, 2021-2022). Analysis and visualization of predicted structures was performed by F.X.V and A.B. on hardware resources supported by the National Institutes of Health under award number NIH SC2GM131992. This work is solely the responsibility of the authors and does not necessarily represent the official views of St. John's University. We want to acknowledge L. Bryan, D. Howarth, T. Mustacchio, M. Ruggiu, and W. Munyao (SJU) for their support and time sharing equipment, reagents, and protocols.

Author contributions

S.J.V. and J.F.J. developed the concepts, conceived of the study plan, and wrote the manuscript. S.J.V. designed and performed the experiments with assistance from S.A.P., V.A.S.E., G.X.C., A.R., A.C.L., E.S.N., P.K., and D.T.S. J.F.J provided project administration, supervision, resources, and data analysis, the latter with V.A.S.E. and S.J.V.'s assistance. A.B. performed 3D structure modeling and analysis of protein interactions under the supervision of F.X.V., who wrote the corresponding section of the manuscript.

Competing interests

The authors declare no competing interests.

bioRxiv preprint doi: https://doi.org/10.1101/2024.06.13.598939; this version posted June 14, 2024. The copyright holder for this preprint (which was not certified by peer review) is the author/funder. All rights reserved. No reuse allowed without permission.

554 **TABLES**

Table 1. Chimeric transcription factors discussed in this work.

Name		TF behaviour		
Common	**Systematic**	**Repressor**	**De-repressible**	**Comments**
Siren	LacI-LNK1-SiaP	Yes	Yes	Functional only in late stationary phase
Sphnx	LacI-LNK2-SiaP	Yes	Yes	Biosensor candidate
Kunst	LacI-LNK3-SiaP	Yes	No	-
Bastet	LacI-LNK5-SiaP	Yes	No	-
Lumos	LacI-LNK6-SiaP	Yes	Yes	Duplicated sequence acts as Linker.
Harpy	LacI-LNK1-SatA	Yes	Unreliable	Unstable strain
Haus	LacI-LNK2-SatA	Yes	No	-

555

Figure 1

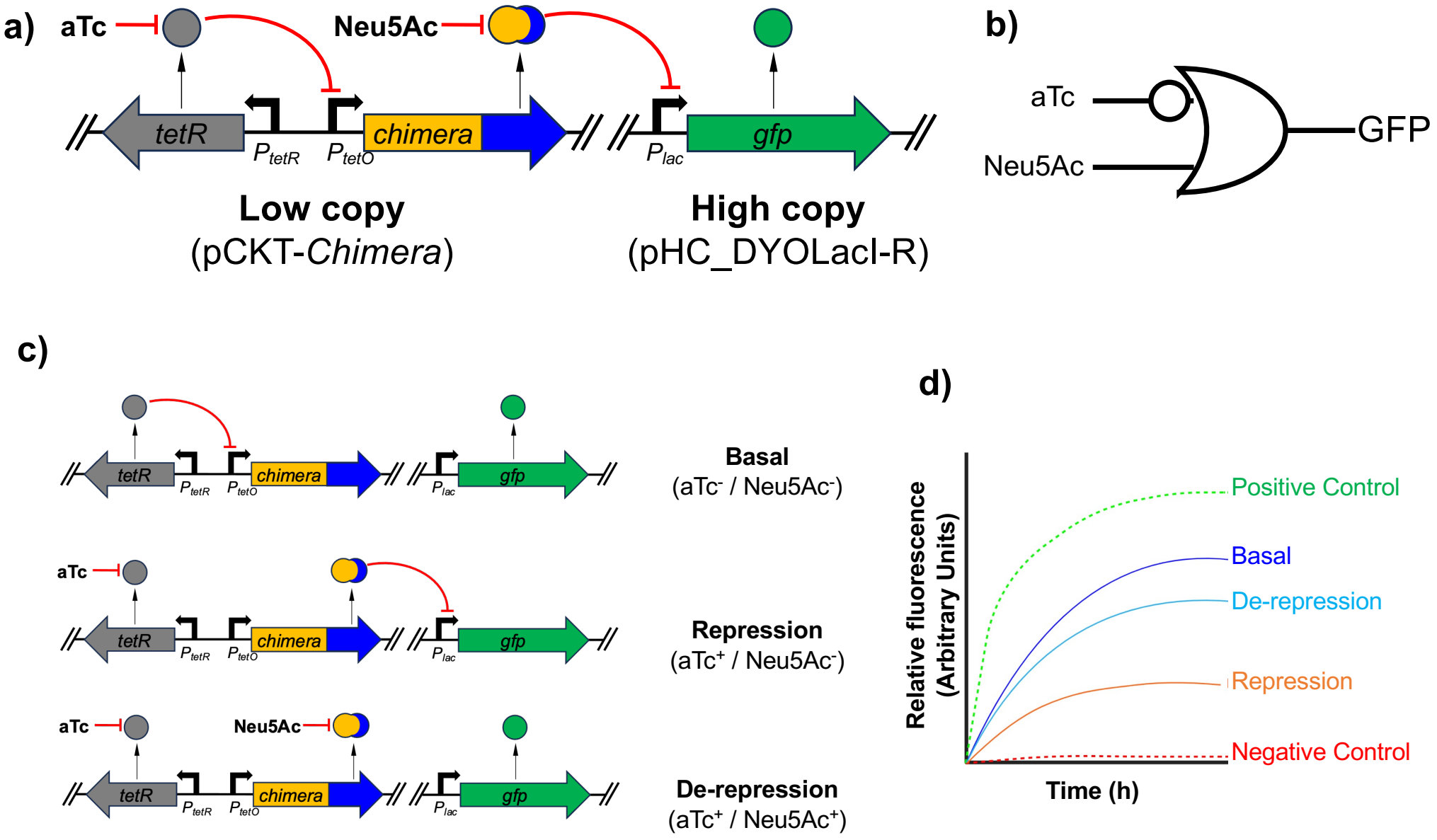
a)
aTc
Neu5Ac
tetR
P_{tetR}
P_{tetO}
chimera
P_{lac}
gfp
Low copy
(pCKT-*Chimera*)
High copy
(pHC_DYOLacI-R)
b)
aTc
Neu5Ac
GFP
c)
Basal
(aTc⁻ / Neu5Ac⁻)
Repression
(aTc⁺ / Neu5Ac⁻)
De-repression
(aTc⁺ / Neu5Ac⁺)
d)
Relative fluorescence
(Arbitrary Units)
Time (h)
Positive Control
Basal
De-repression
Repression
Negative Control

Figure 1. Screening strategy to find functional chimeric transcription factors. a) Biosensor genetic circuit for the *in vivo* testing of the functionality of cloned chimeric TFs. MG1655 (pCKT-*Chimera*, pHC_DYOLacI-R) cells express a chimeric TF under the control of TetR. The chimeric product can repress in *trans* the expression of a GFP reporter unless Neu5Ac is present. *tetR* / TetR (*grey arrow / circle*); chimeric TF gene / protein (*gold-blue arrow / circle*); *gfp* /GFP (*green arrow / circle*); anhydrotetracycline, aTc; neuraminic acid, Neu5Ac. **b)** Standard representation of the B-or-not-A universal two input gate that governs the expression of GFP in the circuit. **c)** States of the biosensor genetic circuit (top to bottom). *Basal*, the absence of aTc (aTc^-) enables TeR to repress the expression of the chimeric repressor: regardless of the presence or absence of Neu5Ac GFP is expressed, and a fluorescent signal is identified. *Repressed*, the presence of aTc (aTc^+) induces TetR which is unable to repress the promoter driving the transcription of the chimeric TF, which in turn represses the promoter driving the expression of *gfp* so that no fluorescent signal is detected. *De-repressed*, the presence of aTc (aTc^+) ensures the production of the chimeric TF which, if functional, gets in turn induced by Neu5Ac, so that it cannot repress *gfp* and the GFP-associated fluorescence is detected again. **d)** Expected profile of fluorescence production over time by a bacterial culture expressing the biosensor genetic circuit and a functional chimeric TF. Relative fluorescence (GFP-associated fluorescence corrected by cell density measured as OD_{600}). *Positive control* (*green line*), corresponds to the maximum GFP-associated fluorescence that can be observed, corresponding to a NEB5-alpha (pHC_DYOLacI-R) strain in which no repressor of the promoter driving GFP expression is present. *Negative control* (*solid red line*), displays background fluorescence by a strain that does not carry *gfp*. *Basal* (*dark blue line*), *Repressed* (*dashed red line*), *De-repressed* (*light blue line*): GFP production associated to a MG1655 (pCKT-*Chimera*, pHC_DYOLacI-R) culture expressing a chimera in the basal, repressed, and de-repressed states, respectively.

Figure 2

a)

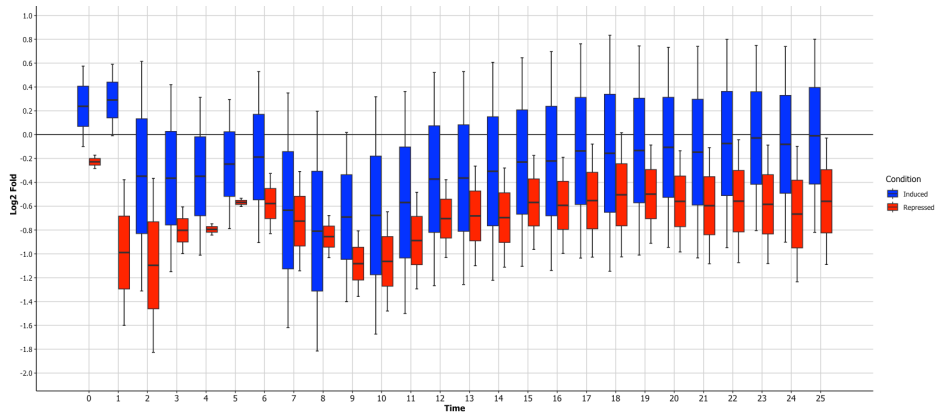
Log2 Fold
Time
Condition
Induced
Repressed

b)

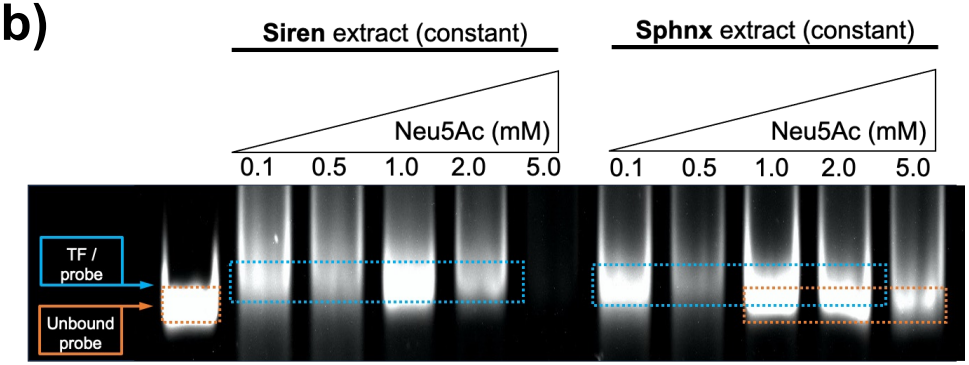
Siren extract (constant)
Sphnx extract (constant)
Neu5Ac (mM)
0.1
0.5
1.0
2.0
5.0
TF / probe
Unbound probe

c)

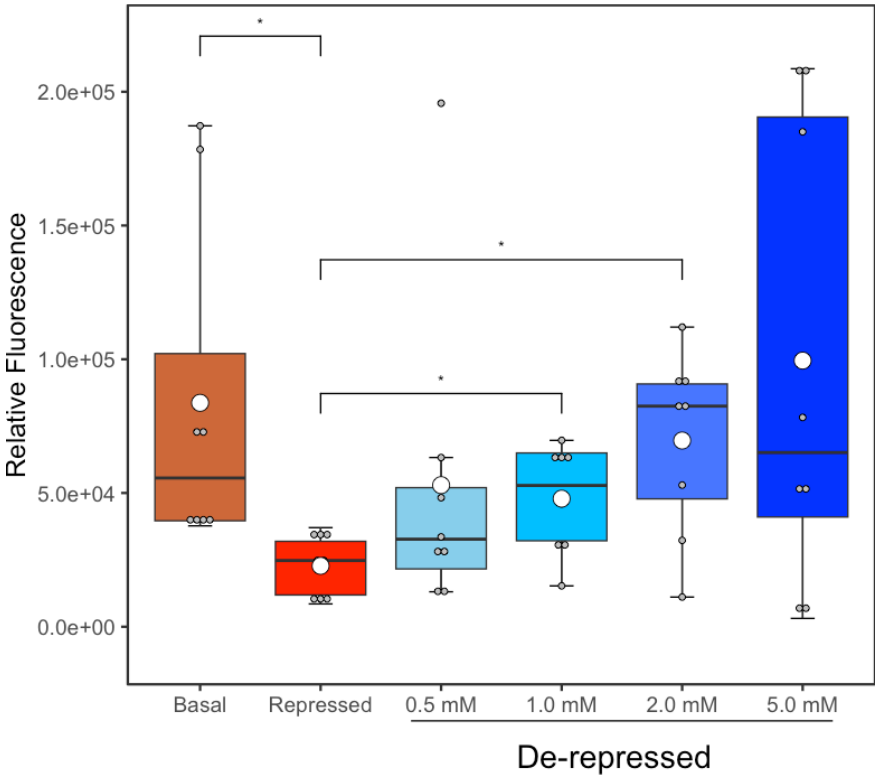
Relative Fluorescence
2.0e+05
1.5e+05
1.0e+05
5.0e+04
0.0e+00
Basal
Repressed
0.5 mM
1.0 mM
2.0 mM
5.0 mM
De-repressed

Figure 2. *V*alidation of the functionality of Sphnx (LacI-LNK2-SiaP). a) Time course showing relative fluorescence of MG1655 (pCKT-Sphnx, pHC_DYOLacI-R) cells grown in a multiwell plate reader over time (hours). Promoter activity is measured as $\log_2$ fold of the relative fluorescence (GFP-associated fluorescence in arbitrary units / OD_{600}) of the strain growing in the de-repressed (aTc^+, $Neu5Ac^+$; *blue boxplots*) or repressed (aTc^+, $Neu5Ac^-$; *red boxplots*) states compared to the basal expression of the reporter (aTc^-, $Neu5Ac^-$). Boxplots with whiskers represent data dispersion of the average values of biological replicas (n = 8). It can be appreciated how in order to approach the basal activity ($\log_2$ fold = 0), the addition of neuraminic acid is necessary when the chimera gets expressed by the supplementation of aTc. Growth conditions and fluorescence assays performed as described in *Materials and Methods*.

b) Sphnx and Siren protein interact with their cognate promoter P_{lac}. EMSA assays were performed as indicated under *Materials and Methods*. Interaction between NEB5-alpha (pCKT-*Chimera*) cell extracts expressing either Sphnx or Siren chimeric TFs and a dsDNA probe (251 bp) including the P_{lac} promoter. A fixed concentration of cell extract and DNA probe was exposed to growing concentrations of neuraminic acid (Neu5Ac). Lane numbers refer to the Neu5Ac concentration (mM) used for each reaction. The positions in the gel associated to unbound and bound probes are identified with orange and blue dashed rectangles, respectively.

c) Relative fluorescence of MG1655 (pCKT-Sphnx, pHC_DYOLacI-R) cultures after induction with different concentrations of neuraminic acid and growth in a multiwell plate reader for 14 hours. Promoter activity is measured as relative fluorescence (GFP-associated fluorescence in arbitrary units / OD_{600}) of the strain growing in the *basal* (aTc^-, $Neu5Ac^-$; *brown*), repressed (aTc^+, $Neu5Ac^-$; *red*) or de-repressed (aTc^+, $Neu5Ac^+$; *blue shades*) conditions. The concentrations of neuraminic acid (mM) added to the de-repressed conditions are specified under the corresponding plots. Boxplots with whiskers represent data dispersion of the average values of biological replicas (n = 8). The average value for every condition corresponds to a white circle. Growth conditions, induction protocol, and fluorescence assays performed as described in *Methods*. Statistically significant differences between selected conditions are marked with stars (p value < 0.05).

Figure 3

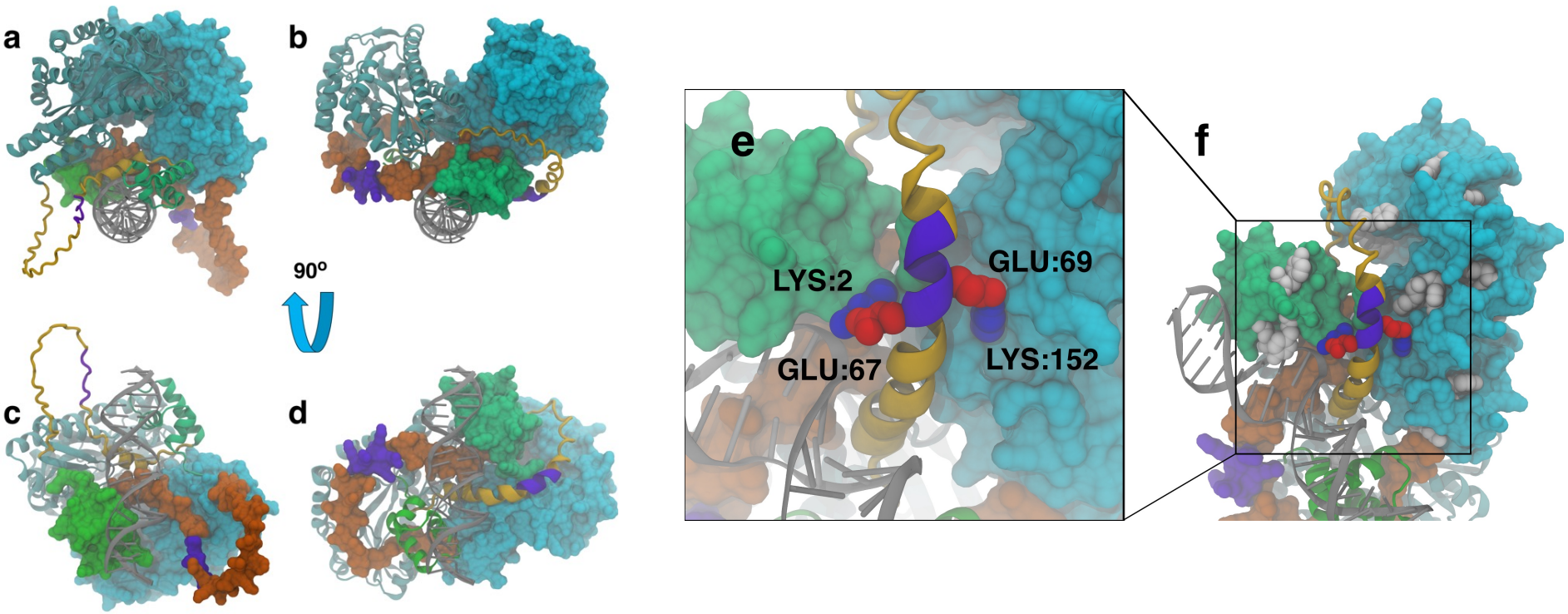

Figure 3. Modeled structures of chimeric protein dimers with double helix DNA obtained with Alphafold 3. For each structure, one monomer is shown using the New Cartoon representation and the other using the space-filling Surf representation. The DBD is shown in *green*, the PBP in *cyan*, and the connecting chain in *orange*, with the engineered linker in *violet*. The Kunst (**a**) and Sphnx (**b**) dimers are shown looking down the axis of the double helix, along with the rotated Kunst (**c**) and Sphnx (**d**) structures. The next panels contain the zoomed-in helical protein (**e**) linker (*violet*) in contact with the DBD (green) and PBP through the formation of salt bridges, with acidic residues shown in red and basic residues in blue. The zoomed-out protein (**f**) highlights the location of aromatic residues (*white*) that can be used to explore the validity of predicted structures using fluorescence anisotropy.

bioRxiv preprint doi: https://doi.org/10.1101/2024.06.13.598939; this version posted June 14, 2024. The copyright holder for this preprint (which was not certified by peer review) is the author/funder. All rights reserved. No reuse allowed without permission.

BIBLIOGRAPHY

1. Pancrazio, J. J., Whelan, J. P., Borkholder, D. A., Ma, W. & Stenger, D. A. Development and application of cell-based biosensors. *Ann. Biomed. Eng.* **27**, 697–711 (1999).
2. Chang, H.-J., Voyvodic, P. L., Zúñiga, A. & Bonnet, J. Microbially derived biosensors for diagnosis, monitoring and epidemiology. *Microb. Biotechnol.* **10**, 1031–1035 (2017).
3. Wu, Y., Wang, C.-W., Wang, D. & Wei, N. A Whole-Cell Biosensor for Point-of-Care Detection of Waterborne Bacterial Pathogens. *ACS Synth. Biol.* **10**, 333–344 (2021).
4. Zhang, F. & Keasling, J. Biosensors and their applications in microbial metabolic engineering. *Trends Microbiol.* **19**, 323–329 (2011).
5. He, W., Yuan, S., Zhong, W.-H., Siddikee, M. A. & Dai, C.-C. Application of genetically engineered microbial whole-cell biosensors for combined chemosensing. *Appl. Microbiol. Biotechnol.* **100**, 1109–1119 (2016).
6. Saltepe, B., Kehribar, E. Ş., Su Yirmibeşoğlu, S. S. & Şafak Şeker, U. Ö. Cellular Biosensors with Engineered Genetic Circuits. *ACS Sens* **3**, 13–26 (2018).
7. Berepiki, A., Kent, R., Machado, L. F. M. & Dixon, N. Development of High-Performance Whole Cell Biosensors Aided by Statistical Modeling. *ACS Synth. Biol.* **9**, 576–589 (2020).
8. Schleif, R. DNA binding by proteins. *Science* **241**, 1182–1187 (1988).
9. Rogers, J. K. *et al.* Synthetic biosensors for precise gene control and real-time monitoring of metabolites. *Nucleic Acids Res.* **43**, 7648–7660 (2015).
10. Juárez, J. F., Lecube-Azpeitia, B., Brown, S. L., Johnston, C. D. & Church, G. M. Biosensor libraries harness large classes of binding domains for construction of allosteric transcriptional regulators. *Nat. Commun.* **9**, 3101 (2018).
11. Koch, M., Pandi, A., Borkowski, O., Batista, A. C. & Faulon, J.-L. Custom-made

bioRxiv preprint doi: https://doi.org/10.1101/2024.06.13.598939; this version posted June 14, 2024. The copyright holder for this preprint (which was not certified by peer review) is the author/funder. All rights reserved. No reuse allowed without permission.

579 transcriptional biosensors for metabolic engineering. *Curr. Opin. Biotechnol.* **59**, 78–84
580 (2019).
581 12. Wren, M. E., Shirtcliff, E. A. & Drury, S. S. Not all biofluids are created equal: chewing
582 over salivary diagnostics and the epigenome. *Clin. Ther.* **37**, 529–539 (2015).
583 13. Bandodkar, A. J. & Wang, J. Non-invasive wearable electrochemical sensors: a review.
584 *Trends Biotechnol.* **32**, 363–371 (2014).
585 14. Campuzano, S., Pedrero, M., Torrente-Rodríguez, R. M. & Pingarrón, J. M. Affinity-based
586 wearable electrochemical biosensors: Natural versus biomimetic receptors. *Anal. Sens.*
587 (2022) doi:10.1002/anse.202200087.
588 15. Omar, E. Current concepts and future of noninvasive procedures for diagnosing oral
589 squamous cell carcinoma--a systematic review. *Head Face Med.* **11**, 6 (2015).
590 16. Wang, S., Yang, M., Li, R. & Bai, J. Current advances in noninvasive methods for the
591 diagnosis of oral squamous cell carcinoma: a review. *Eur. J. Med. Res.* **28**, 53 (2023).
592 17. Haines-Menges, B. L., Whitaker, W. B., Lubin, J. B. & Boyd, E. F. Host Sialic Acids: A
593 Delicacy for the Pathogen with Discerning Taste. *Microbiol Spectr* **3**, (2015).
594 18. Blix, G. Concerning the carbohydrate groups of submaxillary mucin. *Hoppe Seylers Z.*
595 *Physiol. Chem.* **240**, 43–54.
596 19. Lundblad, A. Gunnar Blix and his discovery of sialic acids. Fascinating molecules in
597 glycobiology. *Ups. J. Med. Sci.* **120**, 104–112 (2015).
598 20. Röhrig, C. H., Choi, S. S. H. & Baldwin, N. The nutritional role of free sialic acid, a human
599 milk monosaccharide, and its application as a functional food ingredient. *Crit. Rev. Food*
600 *Sci. Nutr.* **57**, 1017–1038 (2017).
601 21. Vajaria, B. N. *et al.* Salivary glyco-sialylation changes monitors oral carcinogenesis.

bioRxiv preprint doi: https://doi.org/10.1101/2024.06.13.598939; this version posted June 14, 2024. The copyright holder for this preprint (which was not certified by peer review) is the author/funder. All rights reserved. No reuse allowed without permission.

Glycoconj. J. **31**, 649–659 (2014).

22. Phansopa, C. *et al.* Characterization of a sialate-O-acetylesterase (NanS) from the oral pathogen Tannerella forsythia that enhances sialic acid release by NanH, its cognate sialidase. *Biochem. J* **472**, 157–167 (2015).
23. Arthisri, A. S., Sathiyamoorthy, A., Meenakshi, B. & Chandran, C. R. Ratio of Salivary Sialic Acid to Fucose as Tumor Markers in Potentially Malignant Disorders and Oral Cancer. *Contemp. Clin. Dent.* **11**, 131–135 (2020).
24. Chaudhari, V., Pradeep, G. L., Prakash, N. & Mahajan, A. M. Estimation of salivary sialic acid in oral premalignancy and oral squamous cell carcinoma. *Contemp. Clin. Dent.* **7**, 451–456 (2016).
25. Markopoulos, A. K. Current aspects on oral squamous cell carcinoma. *Open Dent. J.* **6**, 126–130 (2012).
26. Coletta, R. D., Yeudall, W. A. & Salo, T. Grand Challenges in Oral Cancers. *Front Oral Health* **1**, 3 (2020).
27. Warnakulasuriya, S. & Greenspan, J. S. *Textbook of Oral Cancer: Prevention, Diagnosis and Management*. (Springer Nature, 2020).
28. Robson, B. Bioinformatics studies on a function of the SARS-CoV-2 spike glycoprotein as the binding of host sialic acid glycans. *Comput. Biol. Med.* **122**, 103849 (2020).
29. Stanton, B. C. *et al.* Systematic transfer of prokaryotic sensors and circuits to mammalian cells. *ACS Synth. Biol.* **3**, 880–891 (2014).
30. Jacob, F. & Monod, J. Genetic regulatory mechanisms in the synthesis of proteins. *J. Mol. Biol.* **3**, 318–356 (1961).
31. Meinhardt, S. *et al.* Novel insights from hybrid LacI/GalR proteins: family-wide functional

bioRxiv preprint doi: https://doi.org/10.1101/2024.06.13.598939; this version posted June 14, 2024. The copyright holder for this preprint (which was not certified by peer review) is the author/funder. All rights reserved. No reuse allowed without permission.

attributes and biologically significant variation in transcription repression. *Nucleic Acids Res.* **40**, 11139–11154 (2012).

32. Fukami-Kobayashi, K., Tateno, Y. & Nishikawa, K. Parallel evolution of ligand specificity between LacI/GalR family repressors and periplasmic sugar-binding proteins. *Mol. Biol. Evol.* **20**, 267–277 (2003).

33. Sakaguchi-Mikami, A., Taniguchi, A., Sode, K. & Yamazaki, T. Construction of a novel glucose-sensing molecule based on a substrate-binding protein for intracellular sensing. *Biotechnol. Bioeng.* **108**, 725–733 (2011).

34. Giuliani, S. E. *et al.* Environment sensing and response mediated by ABC transporters. *BMC Genomics* **12 Suppl 1**, S8 (2011).

35. Locher, K. P. Mechanistic diversity in ATP-binding cassette (ABC) transporters. *Nat. Struct. Mol. Biol.* **23**, 487–493 (2016).

36. Post, D. M. B., Mungur, R., Gibson, B. W. & Munson, R. S., Jr. Identification of a novel sialic acid transporter in Haemophilus ducreyi. *Infect. Immun.* **73**, 6727–6735 (2005).

37. Gruteser, N., Marin, K., Krämer, R. & Thomas, G. H. Sialic acid utilization by the soil bacterium Corynebacterium glutamicum. *FEMS Microbiol. Lett.* **336**, 131–138 (2012).

38. Müller, A. *et al.* Conservation of structure and mechanism in primary and secondary transporters exemplified by SiaP, a sialic acid binding virulence factor from Haemophilus influenzae. *J. Biol. Chem.* **281**, 22212–22222 (2006).

39. Severi, E. *et al.* Sialic acid transport in Haemophilus influenzae is essential for lipopolysaccharide sialylation and serum resistance and is dependent on a novel tripartite ATP-independent periplasmic transporter. *Mol. Microbiol.* **58**, 1173–1185 (2005).

40. Gangi Setty, T., Cho, C., Govindappa, S., Apicella, M. A. & Ramaswamy, S. Bacterial

bioRxiv preprint doi: https://doi.org/10.1101/2024.06.13.598939; this version posted June 14, 2024. The copyright holder for this preprint (which was not certified by peer review) is the author/funder. All rights reserved. No reuse allowed without permission.

periplasmic sialic acid-binding proteins exhibit a conserved binding site. *Acta Crystallogr. D Biol. Crystallogr.* **70**, 1801–1811 (2014).

41. Gangi Setty, T. *et al.* Molecular characterization of the interaction of sialic acid with the periplasmic binding protein from. *J. Biol. Chem.* **293**, 20073–20084 (2018).
42. Oertel-Buchheit, P., Reinbolt, J., John, M., Granger-Schnarr, M. & Schnarr, M. A LexA mutant repressor with a relaxed inter-domain linker. *Protein Sci.* **7**, 512–515 (1998).
43. Tsirigotaki, A., De Geyter, J., Šoštaric, N., Economou, A. & Karamanou, S. Protein export through the bacterial Sec pathway. *Nat. Rev. Microbiol.* **15**, 21–36 (2017).
44. Glick, B. R. Metabolic load and heterologous gene expression. *Biotechnol. Adv.* **13**, 247–261 (1995).
45. Liu, Q., Schumacher, J., Wan, X., Lou, C. & Wang, B. Orthogonality and Burdens of Heterologous AND Gate Gene Circuits in E. coli. *ACS Synth. Biol.* **7**, 553–564 (2018).
46. Logic Gates. *The Department of Mathematics and Computer Science at Oxford College of Emory University* https://mathcenter.oxford.emory.edu/site/cs170/gates/.
47. Lewis, M. The lac repressor. *C. R. Biol.* **328**, 521–548 (2005).
48. Deans, T. L., Cantor, C. R. & Collins, J. J. A tunable genetic switch based on RNAi and repressor proteins for regulating gene expression in mammalian cells. *Cell* **130**, 363–372 (2007).
49. Langdon, R. C., Burr, T., Pagan-Westphal, S. & Hochschild, A. A chimeric activator of transcription that uses two DNA-binding domains to make simultaneous contact with pairs of recognition sites. *Mol. Microbiol.* **41**, 885–896 (2001).
50. Durante-Rodríguez, G. *et al.* Identification of a missing link in the evolution of an enzyme into a transcriptional regulator. *PLoS One* **8**, e57518 (2013).

bioRxiv preprint doi: https://doi.org/10.1101/2024.06.13.598939; this version posted June 14, 2024. The copyright holder for this preprint (which was not certified by peer review) is the author/funder. All rights reserved. No reuse allowed without permission.

671 51. Durante-Rodríguez, G., Mancheño, J. M., Díaz, E. & Carmona, M. Refactoring the λ phage
672 lytic/lysogenic decision with a synthetic regulator. *Microbiologyopen* **5**, 575–581 (2016).
673 52. Oktay, S. *et al.* Serum and saliva sialic acid in periodontitis patients with and without
674 cardiovascular disease. *Pathophysiol. Haemost. Thromb.* **37**, 67–71 (2010).
675 53. Snoek, T. *et al.* Evolution-guided engineering of small-molecule biosensors. *Nucleic Acids*
676 *Res.* **48**, e3 (2020).
677 54. Hebisch, E., Knebel, J., Landsberg, J., Frey, E. & Leisner, M. High variation of
678 fluorescence protein maturation times in closely related Escherichia coli strains. *PLoS One*
679 **8**, e75991 (2013).
680 55. Chen, X., Zaro, J. L. & Shen, W.-C. Fusion protein linkers: property, design and
681 functionality. *Adv. Drug Deliv. Rev.* **65**, 1357–1369 (2013).
682 56. Abramson, J. *et al.* Accurate structure prediction of biomolecular interactions with
683 AlphaFold 3. *Nature* (2024) doi:10.1038/s41586-024-07487-w.
684 57. Meuzelaar, H., Vreede, J. & Woutersen, S. Influence of Glu/Arg, Asp/Arg, and Glu/Lys
685 Salt Bridges on α-Helical Stability and Folding Kinetics. *Biophys. J.* **110**, 2328–2341
686 (2016).
687 58. Raman, S., Taylor, N., Genuth, N., Fields, S. & Church, G. M. Engineering allostery.
688 *Trends Genet.* **30**, 521–528 (2014).
689 59. Levine, M. J. Development of artificial salivas. *Crit. Rev. Oral Biol. Med.* **4**, 279–286
690 (1993).
691 60. Persico, M. *et al.* From Protein Communication to Drug Discovery. *Curr. Top. Med. Chem.*
692 **15**, 2019–2031 (2015).
693 61. Bertani, G. Lysogeny at mid-twentieth century: P1, P2, and other experimental systems. *J.*

bioRxiv preprint doi: https://doi.org/10.1101/2024.06.13.598939; this version posted June 14, 2024. The copyright holder for this preprint (which was not certified by peer review) is the author/funder. All rights reserved. No reuse allowed without permission.

694 *Bacteriol.* **186**, 595–600 (2004).

695 62. Miller, J. H. *Experiments in Molecular Genetics*. (1972).

696 63. Sambrook, J. & Russell, D. W. *Molecular Cloning: A Laboratory Manual*. (CSHL Press,

697 2001).

698 64. Sanger, F., Nicklen, S. & Coulson, A. R. DNA sequencing with chain-terminating

699 inhibitors. *Proc. Natl. Acad. Sci. U. S. A.* **74**, 5463–5467 (1977).

700 65. Gibson, D. G. *et al.* Enzymatic assembly of DNA molecules up to several hundred

701 kilobases. *Nat. Methods* **6**, 343–345 (2009).

702 66. Yanisch-Perron, C., Vieira, J. & Messing, J. Improved M13 phage cloning vectors and host

703 strains: nucleotide sequences of the M13mp18 and pUC19 vectors. *Gene* **33**, 103–119

704 (1985).

705 67. Livak, K. J. & Schmittgen, T. D. Analysis of relative gene expression data using real-time

706 quantitative PCR and the 2(-Delta Delta C(T)) Method. *Methods* **25**, 402–408 (2001).

707 68. Humphrey, W., Dalke, A. & Schulten, K. VMD: visual molecular dynamics. *J. Mol. Graph.*

708 **14**, 33–8, 27–8 (1996).

709